SPE 59313

An Improved Three Phase Flow Model Incorporating Compositional Variance

F.J.Fayers SPE and A.P.Foakes, BP Amoco, and C.Y.Lin, BP Amoco and D.A.Puckett SPE, BP Amoco

This paper was prepared for presentation at the 2000 SPE/DOE Improved Oil Recovery Symposium held in Tulsa, Oklahoma, 3–5 April 2000.

Abstract

A consistent set of procedures for calculating 3 phase relative permeabilities (3PRPs) and the capillary pressures (3PCPs), referred to as the rescaled Interpolation Method (RIM), is described. The intention is to provide an approach for mixed-wet systems which is compatible with the likely availability of immiscible 2P measured data, which honours the basic physics of 3P displacement processes, and at the same time avoids undue complexity in the simulator and excessive overheads in computing efficiency. For 3PRPs the starting point rests on the use of the Baker saturation weighted interpolation method for the three phases, but modified for the oil phase through saturation rescaling to give compatibility with a general form for the residual saturation function $S_{om}(S_g,S_w)$. Comparisons with experimental data show the benefits of this approach as opposed to Stone's I. A practical procedure for including 3P hysteresis is described. This is then extended to allow for compositional changes in the oil and gas phases, including the limiting miscibility conditions. The model for 3PCPs is based on simple assumptions concerning the division of the pore space between water-wet and oil-wet pores and comparing this with the phase occupancies of pores in the corresponding 2PCP-measurements. The mixed-wet pore space division is found from the cross over saturation in the water/oil 2PCP.

Introduction

Gas injection is becoming a significant process for IOR opportunities. Compositional simulation is necessary to optimize the gas injection strategy, where a primary economic consideration is often the implications of different choices on levels of gas enrichment. It has become recognised that a process designed to be multi-contact miscible will not achieve miscibility in the reservoir due to physical dispersion effects[1,2], and that reduction of enrichment may give a more economically attractive project. This places a major emphasis on the quality of the three-phase flow approximations in the simulator, since these have increasing importance as the enrichment is reduced. Furthermore, fine scale grids and detailed reservoir descriptions are now used in modern compositional simulations, and these can imply the need for adequate accuracy in both the 3 phase relative permeabilities (3PRPs) and the 3 phase capillary pressures (3PCPs). Unfortunately, there is a severe lack of reliable measurements or theoretical models on 3PRPs and 3PCPs, so there is a tendency to adopt complicated correlations in the simulators with a multitude of non-physical parameters, for which the user has little information to guide selection of the values appropriate to his reservoir. This position is further intensified when hysteresis in flow and compositional changes to the phases occur, both of which can be very significant in a WAG injection application.

This paper provides details of a logical framework for computing both 3PRPs and 3PCPs in mixed-wet systems in the context of changing oil and gas compositions and with hysteresis. The intention is to provide an approach which is compatible with the likely availability of immiscible 2P measured data, which honors some elementary physics in 3P displacement processes, but at the same time avoids undue complexity in the simulator and excessive overheads in computing efficiency. We have deliberately made compromises by exercising judgements on the modeling details and have omitted some effects which were deemed to be less important in their consequences, or for which there were unlikely to be reliable measurements to allow determination of their parameters. Part of the intention was that the formulation should be transparent from the standpoint of user understanding and degree of approximation.

For 3PRPs the starting point rests on the use of the Baker saturation weighted interpolation method for the oil, water and gas phases, but modified for the oil phase through saturation rescaling to give compatibility with a general form for the residual $S_{orm}(S_g)$ function (symbol definitions are given in the Nomenclature). A practical procedure for including hysteresis is described. This is then extended to allow for compositional changes in the oil and gas phases, including the limiting

miscibility conditions. The model for 3PCPs is based on simple assumptions concerning the division of the pore space between water-wet and oil-wet pores, and comparing this with the phase occupancies of pores in the corresponding 2PCP measurements. We show some comparisons between the recommendations of this paper and the more conventional forms used for 3P flow correlations, and comment on the accuracy implications from some of the very limited experimental information.

Procedures for Basic Immiscible Three Phase Relative Permeabilities

The underlying approach we will advocate at each stage of this presentation is the use of linear interpolation methods with saturation rescaling to comply with selected residual saturations. We assume that tabular measured data are available as input for 2P k_r for water/oil, gas/oil, and water/gas systems, where the last two are made with connate water saturation. S_{wc} is regarded as a fixed irreducible water saturation. The values of S_{orw} and S_{org} are key parameters and particular care is needed to obtain an accurate value for S_{org}. The k_r measurements should ideally be made at reservoir conditions with appropriate rock wettability. We will assume for this discussion a mixed-wet porous medium, although the generalisation of the concepts to preferentially water-wet or oil-wet conditions is not difficult. If the basic input data have not been measured, the user is obliged to exercise judgment in estimating the missing data, e.g. using $k_{rwg}(S_w) \sim k_{rog}(1\text{-}S_g)$.

The popular method used in most codes for estimating 3P k_{ro} is the non-linear Stone's method I with linear interpolation of S_{om}[3]. In a recent paper analysing the mathematical properties of Stone's I (see Balbinski et al[4]) reservations are expressed about its mathematical properties. We summarise our views on these concerns in Appendix 1. An alternative simpler form introduced by Baker[5] is the linear interpolation model. We modify this form by introducing saturation rescaling to give the equation:

$$k_{ro}\left(S_w, S_g\right) = \left(1 - S_{gw}\right) k_{row}^{m}\left(S_o^{rw}\right) + S_{gw} k_{rog}^{m}\left(S_o^{rg}\right) \quad \text{.....(1)}$$

Superscript *m* refers to measured. The interpolation weight S_{gw} is given by:

$$S_{gw} = S_g \big/ \left(S_w + S_g - S_{wc}\right) \quad \text{.....(2)}$$

The rescaled saturations S_o^{ri} are defined by:

$$S_o^{ri} = r_i S_o + \left(1 - r_i\right)\left(1 - S_{wc}\right) \quad \text{..... } i = w, g \text{ .....(3)}$$

where the rescaling parameters r_i are given by:

$$r_i = \left(1 - S_{ori} - S_{wc}\right) \big/ \left(1 - S_{om} - S_{wc}\right) \quad \text{..... } i = w, g \text{ .....(4)}$$

$S_{om}(S_g,S_w)$ is the residual oil saturation, for which we might expect $S_{org} \le S_{om} \le S_{orw}$. This then implies $r_w \le 0$ and $r_g \ge 1$. The rescaling relations above are applied to the current 3P oil saturation S_o, and cause both k_{row} and $k_{rog} \to 0$ when $S_o \to S_{om}$.

For $S_o >> S_{om}$, the saturation rescalings have only a small effect. The important region governing oil recovery potential from gas injection is for $S_o \sim S_{om}$. Due to the almost complete absence of reliable data on S_{om} (particularly for mixed-wet conditions), we have suggested the following general relation:

$$S_{om} = \alpha S_{org} + (1-\alpha) S_{orw} + S_g\left(S_w - S_{wc}\right)\left(\beta S_{orw} - a S_{gt}\right) \text{.....(5)}$$

where:

$$\alpha = S_g \big/ \left(1 - S_{wc} - S_o\right) \text{.....(6)}$$

This definition of S_{om} fulfils the necessary conditions $r_g = 1$ when $S_w = S_{wc}$ and $r_w = 1$ when $S_g = 0$. By selecting $\beta = 0$ and $a = 0$ we obtain a nearly linear form for S_{om}, slightly different from that often used in Stone's I (Appendix 1). Choosing $\beta < 0$ implies a convex curvature favorable for gas displacement, while $\beta > 0$ gives an unfavorable concave curvature. The optional input parameter a recognises that trapped gas saturation S_{gt} can reduce residual oil saturation, particularly for more water-wet conditions[3]. This rescaled interpolation method (RIM) has more realistic convergence properties as $S_o \to S_{om}$ compared with Stone's I (Appendix 1), and also has its look-up saturation for k_{row} and k_{rog} more intuitively based on S_o, rather than S_w and S_g used in Stone's I.

Isoperms in ternary diagrams for RIM with $\beta = a = 0$ are compared with Stone's I in Figures 1 and 2, for two different sets of 2P field k_r's (parameterised as per Appendix 2). The differences at low oil saturations are noticeable, although they converge to almost the same linear forms for S_{om}. The RIM isoperms for $S_o \sim S_{om}$ and $S_g \sim 1\text{-}S_{wc}$ for Field 1 data set (Fig 1) show a tendency to curl upwards, for which we will comment later. Shown in Figs 3 and 4 are comparisons with isoperms obtained from the 3P measurements of Hossain[6] and Saraf et al[7]. These two sets were regarded as the most reliable of older measurements in Ref (3), where the isoperm fits were interpolated from the measured data. They apply to water-wet conditions. The excellent RIM matches in Figs 3 and 4 were calculated with $\beta = 2$ and $\beta = -1$ respectively, but good results are also given from $\beta = 0$. The corresponding results[3] using Stone's I have less satisfactory curvatures at high oil saturation. Measurements for an intermediate-wet Berea core have been reported by Oak[8], for which the isoperm comparison with RIM is shown in Fig 5. These experiments indicate very unfavorable conditions for gas injection ($S_{orw} = 0.27$, $S_{org} = 0.28$, and a strongly adverse convex curvature). The excellent RIM match required $\beta = 8.0$, with noticeably less satisfactory results from $\beta = 0$. The corresponding Stone's I predictions are shown in Fig 5b, which give a very misleading picture for gas displacement in this system. We regard the degree of agreement with RIM for all the above experiments as very satisfactory, but note that the errors in the measured isoperms are large at low oil saturation because of scarcity of data points in this region (particularly in the important area of larger gas saturation). Some 3P

measurements in reservoir cores would be desirable to confirm the appropriate value of β in a field application.

For mixed-wet conditions, we suggest that both k_{rw} and k_{rg} are not uniquely determined as functions of their own saturation, contrary to assumptions in the Stone's methods for water-wet systems. We therefore use linear interpolation equivalents of Eq. (1) in the form:

$$k_{rw}\left(S_w, S_g\right) = S_{og} k_{rwo}^{m}\left(S_w\right) + \left(1 - S_{og}\right) k_{rwg}^{m}\left(S_w\right) \quad \text{.....(7)}$$

$$k_{rg}\left(S_w, S_g\right) = S_{ow} k_{rgo}^{m}\left(S_g\right) + \left(1 - S_{ow}\right) k_{rgw}^{m}\left(S_w\right) \quad \text{.....(8)}$$

where:

$$S_{og} = S_o \Big/ \left(S_o + S_g\right)$$

$$S_{ow} = S_o \Big/ \left(S_o + S_w - S_{wc}\right)$$

There are no saturation rescalings in Eq. (7) because the water saturation limits for 3P-flow are S_{wc} and 1. $k_{rw}^{m}(1) \rightarrow 1$ has to be included because of oil vaporisation effects. For k_{rg}, the S_g limits are 1 - S_{wc} and S_{gt}. S_{gt} is discussed in the next section. We note that Eq. (8) gives the Stone's result $k_g = k_{rgo}^{m}(S_g)$, if it is assumed that $k_{rgw}^{m}(S_g) = k_{rgo}^{m}(S_g)$, but the latter is not necessarily valid for a mixed-wet system.

Inclusion of Hysteresis Effects

There are 12 possible hysteresis classes in 3P flow. Using I,D,T to denote increasing, decreasing, trapped, and listing in the order *w,g,o* the possible combinations are IID,IDI,IDD,IDT,ITD,TID,TDI,DII,DID,DIT,DTI,DDI. The standard two-phase measurements provide I-D for the water/oil system and TID for the gas/oil system. We make some sweeping simplifying assumptions in our treatment of 3P hysteresis. We assume for each phase that its hysteresis is governed by whether that phase is increasing or decreasing, regardless of the state of the other phases. We regard gas as being essentially non-wetting (in spite of the arguments about wetting films and contact angles[9]) and that there is a good estimate for the maximum trapped gas S_{gtm}. The latter is taken to be independent of whether water or oil are the displacing phases. For the water/oil system we suggest the need for the measurement of the bounding secondary drainage curves under proper conditions starting from S_{orw} (we have not seen such data for mixed-wet reservoir rock and real fluids). We assume that S_{orw} will not change under a further reversal to a tertiary imbibition, and that hysteresis in 3P k_{ro} is governed by the 2P water/oil behavior.

The current trapped gas saturation S_{gr} during secondary imbibition is given by:

$$S_{gr} = \left[\left(S_{g\max} - S_g\right)\left(S_{gt} - S_{gc}\right) \Big/ \left(S_{g\max} - S_{gt}\right)\right] + S_{gc} \quad \text{.....(9)}$$

where $S_{g\max}$ is the historic maximum S_g and S_{gt} is the terminal trapped gas saturation that will be achieved on the current hysteresis cycle:

$$S_{gt} = \left[\left(S_{gtm} - S_{gc}\right)\left(S_{g\max} - S_{gc}\right) \Big/ \left(1 - S_{wc} - S_{gc}\right)\right] + S_{gc} \quad \text{.(10)}$$

The gas relative permeability curves k_{rgo} and k_{rgw} are then rescaled to satisfy the current value of S_{gr}, that is:

$$k_{rgi}^{h} = k_{rgi}^{m}\left(S_g^{h}\right) \quad \text{..... } i = w, o \text{ .....(11)}$$

and:

$$S_g^{h} = \left[\left(S_g - S_{gr}\right)\left(1 - S_{wc} - S_{gc}\right) \Big/ \left(1 - S_{wc} - S_{gc}\right)\right] + S_{gc} \quad \text{..(12)}$$

Fig 6 shows a schematic example of the method. Note that only the values of the current 3P S_g and $S_{g\max}$ are involved, with the input data S_{gc} and S_{gtm}.

Hysteresis in k_{ro} and k_{rw} are computed from the bounding water/oil curves for secondary drainage and imbibition illustrated in Figs 7a and b. The hysteresis paths depend respectively on the 3P values of $S_{o\min}$ and $S_{w\max}$ previously reached, and on the current 3P values S_o and S_w. Using superscript *h* to denote hysteresis:

$$k_{rwo}^{h} = r_w^{h} k_{rwo}^{mi}\left(S_w\right) + \left(1 - r_w^{h}\right) k_{rwo}^{md}\left(S_w\right) \quad \text{.....(13)}$$

$$k_{row}^{h} = r_o^{h} k_{row}^{mi}\left(S_o\right) + \left(1 - r_o^{h}\right) k_{row}^{md}\left(S_o\right) \quad \text{.....(14)}$$

where the interpolation weights are given by:

$$r_w^{h} = \frac{\left(1 - S_{w\max} - S_{orw}\right) S_w}{\left(1 - S_{w\max} - S_{orw}\right) S_w + \left(S_{w\max} - S_w\right)\left(S_{w\max} - S_{wc}\right)} \quad \text{.....(15)}$$

$$r_o^{h} = \frac{\left(S_{o\min} - S_{orw}\right)\left(1 - S_o\right)}{\left(S_{o\min} - S_{orw}\right)\left(1 - S_o\right) + \left(S_o - S_{o\min}\right)\left(1 - S_{o\min} - S_{wc}\right)} \quad \text{.(16)}$$

Eqs. (13) and (15) satisfy the requirements that when $S_w = S_{wmax}$, $k_{rwo}^{h} = k_{rwo}^{mi}$, and when $S_{wmax} = 1 - S_{orw}$, $k_{rwo}^{h} = k_{rwo}^{md}$. Similar arguments apply to Eqs. (14) and (16).

If hysteresis is occurring, the above results can be used as replacements for the k_r^{m} values in the 3P linear interpolation equations of the previous section. However, we first need to consider compositional effects, which are discussed next.

Inclusion of Compositional Effects

Phase behaviour will cause changes to the oil and gas compositions, so that if the system is approaching miscibility, these two phases will tend towards the same compositions. However, dispersion effects will cause loss of multiple contact miscibility[1,2], and the eventual state of the phases depends on the type of process. For a condensing process, both oil and gas phases become lighter, whereas for vaporising processes oil and gas both become heavier. For the commonly occurring condensing/vaporising mechanism, the vaporising mechanism

prevails to leave a heavy oil residue and a heavier gas. There seems to be no information on how 2PRPs will change as a function of the phase compositions. Thus, we have elected to use the simplest plausible model. The compositional changes are determined by three regions. The strictly immiscible region uses values of k_r^m or k_r^h without further changes, while the compositional region mixes oil/water and gas/water 2P k_r according to mass fractions of gas in the oil phase, and gas in the gas phase. The third region involves phase behaviour fairly close to miscible, with a limit at complete miscibility.

For the compositional region we evaluate the mass fractions of gas in a phase, α_{go} and α_{gg}, from relations of the form:

$$\rho_i = \alpha_{gi}\rho_g^m + \left(1-\alpha_{gi}\right)\rho_o^m \quad \ldots\ldots\ldots\ldots\ldots\ldots\ i = w,g \quad \ldots\ldots (17)$$

where the ρ_i are the current phase densities and the α are constrained to lie in the range 0 to 1. The bounding phase densities ρ_g^m and ρ_o^m are input parameters controlling when the compositional region commences for the oil and gas phases, independently. A default selects these parameters as the average initial densities for reservoir oil and equilibrium gas. Note that an option allows selection of smaller values for ρ_o^m and larger values for ρ_g^m which delay the onset of the compositional region. The input k_r^m must be selected from measurements valid for the immiscible region. The compositionally mixed equations for k_{riw}^c are again evaluated from interpolation and saturation rescaling:

$$S_{orw}^c = \alpha_{go}S_{gt} + \left(1-\alpha_{go}\right)S_{orw} \quad \ldots\ldots\ldots\ldots\ldots\ldots\ldots\ldots\ldots\ldots (18)$$

$$S_{gt}^c = \alpha_{gg}S_{gt} + \left(1-\alpha_{gg}\right)S_{orw} \quad \ldots\ldots\ldots\ldots\ldots\ldots\ldots\ldots\ldots\ldots (19)$$

$$k_{riw}^c\left(S_i\right) = \alpha_{gi}k_{rgw}^h\left(S_i^{rg}\right) + \left(1-\alpha_{gi}\right)k_{row}^h\left(S_i^{ro}\right) \ldots i = g,o \ldots\ldots (20)$$

The saturation rescalings required for S_o^{rg} and S_o^{ro} are achieved by similar relations to those given in Eq (3) and (4), but using the values of S_{orw}^c and S_{gt}^c from Eqs. (18) and (19) in Eq. (5). Similarly for k_{rwi}^c (i = g,o) we use:

$$k_{rwi}^c\left(S_w\right) = \alpha_{gi}k_{rwg}^m\left(S_w\right) + \left(1-\alpha_{gi}\right)k_{rwo}^h\left(S_w\right) \ldots i = g,o \ldots\ldots (21)$$

for which there are no saturation rescaling requirements. Hysteresis values or the measured values are used in Eqs.(20) and (21) depending on the hysteresis mode of the respective phases.

For gas/oil 2PRPs, there are usually no experimental data or theoretical guidelines to suggest a useful form for compositional dependence. We therefore assume there is no dependency until entry to the near miscible behavior in the third region. Finally, the compositional 3P results are obtained from applying Eqs. (1) to (6) using the appropriate compositional 2PRPs. Fig 8 shows a compositionally modified form of Fig 1 for k_{ro} in which the compositional mass fractions were $\alpha_{gg} = 0.7$ and $\alpha_{go} = 0.3$. There are significant compositional changes for this data set, mainly driven by the shape of the hysteresis curve for k_{rgw}. The compositional changes for the Field 2 data in Fig 2 are much less dramatic.

The near-miscible third region is dealt with by requiring the 3PRPs to converge uniformly to the correct forms at the miscible limit. The boundary of the third region is determined from an input critical capillary number N_{goc}, where :

$$N_{go} = \sigma_{go}k_{rg}\big/\left(\mu_g\, q_g\right) \quad \ldots\ldots\ldots\ldots\ldots\ldots\ldots\ldots\ldots\ldots\ldots\ldots (21)$$

q_g is the Darcy flow rate of gas. The limiting miscible relations are :

$$k_{ro}^{mi} = \left[\left(S_o - S_{obw}\right)\big/S_{of}\right]k_{rhw} \quad \ldots\ldots\ldots\ldots\ldots\ldots\ldots\ldots\ldots\ldots (22)$$

$$k_{rg}^{mi} = \left(S_g\,/S_{of}\right)k_{rhw} \quad \ldots\ldots\ldots\ldots\ldots\ldots\ldots\ldots\ldots\ldots\ldots\ldots (23)$$

where:

$$S_{of} = S_o + S_g - S_{obw}$$

and $S_{obw}(S_w)$ is a water blocking function. The relative permeability of hydrocarbon to water is given by:

$$k_{rhw}\left(S_w\right) = \alpha_{gh}k_{rgw}^m\left(S_w^{hg}\right) + \left(1-\alpha_{gh}\right)k_{row}^h\left(S_w^{ho}\right) \quad \ldots\ldots\ldots\ldots (24)$$

with a similar equation for k_{rwh}. The saturation rescalings of the 3P S_w in Eq.(24) are based on the hydrocarbon residual saturation:

$$S_{hrw} = \alpha_{gh}\left(S_{gt} + S_{obw}\right) + \left(1-\alpha_{gh}\right)S_{orw} \quad \ldots\ldots\ldots\ldots\ldots\ldots (25)$$

The inclusion of S_{obw} in the first term of Eq. (25) ensures that $S_{hrw} \to S_{gt} + S_{obw}$ when $\alpha_{gh} \to 1$. The gas mass fraction in the near miscible region is obtained from:

$$\alpha_{gh}\rho_g^m + \left(1-\alpha_{gh}\right)\rho_o^m = \frac{\left(S_o - S_{obw}\right)\rho_o + S_g\rho_g}{S_o - S_{obw} + S_g} \quad \ldots\ldots\ldots\ldots (26)$$

Uniform convergence from compositional conditions in region 2 to the miscible limit of region 3 are obtained using the relations:

$$k_{ri}^{nm} = r_m k_{ri}^c + \left(1-r_m\right)k_{ri}^{mi} \quad \ldots\ldots\ldots\ldots\ldots i = g,o,w \quad \ldots\ldots (27)$$

where

$$r_m = \left(N_{go}\,/N_{goc}\right)^n \quad \ldots\ldots\ldots\ldots\ldots\ldots\ldots\ldots\ldots\ldots\ldots\ldots\ldots\ldots (28)$$

Fig 9 compares with Fig 8 for a case with $\alpha_{gh}(S_o,S_g)$ calculated from Eqs. (17) and (26) and with $r_m = 0.5$.

A Simple Model for Phase Distributions and 3PCPs

We postulate a simple model of wettability distribution and its consequences for 3PCPs, and also to allow comment on the

implications for 3PRPs. The mixed-wet system is envisioned to have a range of smaller pores which are water-wet, and an upper range of larger pores which are oil-wet. For 2P flow, the water/oil contact angle can continuously increase as the pore size occupancy by water increases. The imbibition filling sequence by water is to first flood all the smaller pores, and then to flood the largest pores in the oil-wet space. The immobile connate water is regarded as being irreducibly trapped in the smallest water-wet pores. The mixed-wet behavior is indicated by the positive and negative portions of the 2P P_{cwo} curve shown in Fig 10a, and the cross over saturation S_{ww} at $P_{cwo} = 0$ defines the position of change of wettability. For the 2P gas/oil system measured at S_{wc}, the P_{cgo} curve in Fig 10b is usually not seen to have any sign change, and gas is therefore declared to be non-wetting. This implies a uniform pore filling sequence for gas from largest to smallest pores. Gas is also assumed non-wetting to water. A consequent 3P saturation distribution for $S_w > S_{ww}$ is shown in Fig 11a, with the corresponding distributions for water and gas in Figs 11b and 11c for the related 2P measurement conditions where the 3P S_o is the look up variable. The figures show pore size occupancies for a double porosity distribution. This implies that in Eq. (1) for the 3P k_{ro}, the oil in the 2P gas/oil measurement occupies pores which are too small. However, the weighting of the k^m_{row} term is fairly dominant for this case. Corresponding distributions for $S_w < S_{ww}$ and at high gas saturation are displayed in Fig 12. A similar error is involved in the oil occupancy from the gas/oil k_r measurement, but its effects at low oil saturations could be more significant than in the previous case. Eventually, we must have $k_{ro} \rightarrow k^m_{rog}$ when $S_w \rightarrow S_{wc}$. Therefore we might expect that the real isoperms could have the kind of shape near $S_w \sim S_{wc}$ predicted by RIM in Fig 1. Also under these conditions, the presence of some mobile water in a water-wet region could promote the development of oil films, which could also locally increase k_{ro}.

The simple models of phase occupancies of pores for 3P saturation distributions lead to relations for P_c. This is done more readily because the P_c values depend on a simple pore throat size analogy (i.e. $P_{cwo} = 2\sigma_{wo} \cos\theta_{wo}/r_{wo}$ in which r_{wo} is the next pore throat radius to be invaded), whereas k_r depend on integrals over pore sizes. The sequences are shown in Figs 13 and 14, where the 3P values of S_w and S_g become the look up variables. Using the 2P and 3P pore occupancy comparisons and the critical throat size analogy, we obtain the following results:

For $S_w > S_{ww}$:

$$P^3_{cwo}\left(S_w, S_g\right) = P^m_{cwo}\left(S_w + S_g\right) \quad \text{.....(29)}$$

For $S_w < S_{ww}$, r_{wo} depends only on S_w, thus:

$$P^3_{cwo}\left(S_w, S_g\right) = P^m_{cwo}\left(S_w\right) \quad \text{.....(30)}$$

For the 3P P_{cgo}, the oil and gas phases in Fig 13a are separated by an oil/water interface at r_{wo}, and by a water/gas interface at r_g, i.e. a double displacement mechanism. Hence, for $S_w > S_{ww}$:

$$P^3_{cgo}\left(S_w, S_g\right) = P^m_{cgw}\left(S_g\right) - P^m_{cwo}\left(S_w + S_g\right) \quad \text{.....(31)}$$

For $S_w < S_{ww}$, in Fig 14a, there is a direct gas/oil contact, so that:

$$P^3_{cgo}\left(S_w, S_g\right) = P^m_{cgo}\left(S_g\right) \quad \text{.....(32)}$$

We note that from the definition of capillary pressure ($P_{cgw} = P_g - P_w$), there follows for $S_w > S_{ww}$:

$$P^3_{cgw}\left(S_w, S_g\right) = P^3_{cwo}\left(S_w, S_g\right) + P^3_{cgo}\left(S_w, S_g\right) = P^m_{cgw}\left(S_g\right) \quad \text{....(33)}$$

but for $S_w < S_{ww}$:

$$P^3_{cgw}\left(S_w, S_g\right) = P^m_{cwo}\left(S_w\right) + P^m_{cgo}\left(S_g\right) \quad \text{.....(34)}$$

In Fig 15a, $P_{cwo}(S_w,S_g)$ obtained from Eqs. (29) and (30) with $S_{ww} = 0.33$ may be compared with the usual assumption of $P^m_{cwo}\left(S_w\right)$, shown in Fig (10a). Fig 15b shows $P^3_{cgo}\left(S_w, S_g\right)$ calculated from Eqs. (31) and (32) in a case of low P_{cgo} which can be compared with $P^m_{cgo}\left(S_g\right)$ in Fig 10b. The sharp change implied by Fig 15b at S_{ww} is due to the differences in the magnitude of the capillary pressure across the different interfaces and will disappear when $P^3_{cgo} \rightarrow 0$ as the miscible limit is approached (see Eq. 39 below). The occurrence of sharp changes in 3P P_c has also been suggested from the work of van Dijke et al[9], who studied a mixed-wet capillary bundle model with wetting angles related to the presence of wetting films.

The question of hysteresis in 3P P_c is difficult, particularly in view of the existence of the twelve hysteresis classes referred to previously. For P_c, our proposal is to regard water and gas as the primary driving phases and to relate hysteresis in P_c to $S_{w\max}$ and $S_{g\max}$ regardless of the direction of the changes in S_o. This then allows the Killough model[10] to be used with the necessary measured P_c bounding curves, shown in Figs 10a and 10b. The scanning curve is calculated from the Killough equation:

$$P^h_{coi}\left(S_i\right) = P^m_{cio}\left(S_i\right) + \left(\frac{\dfrac{1}{S_{i\max} - S_i + \varepsilon_i} - \dfrac{1}{\varepsilon_i}}{\dfrac{1}{S_{i\max} - S_{ic} + \varepsilon_i} - \dfrac{1}{\varepsilon_i}}\right)\left[P^m_{coi}\left(S_i\right) - P^m_{cio}\left(S_i\right)\right] \quad \ldots\ i = w, g \quad \text{....(35)}$$

where ε_i is an input parameter affecting the shape of the scanning curve. Recommended values are 0.05 to 0.1. In view of other uncertainties in evaluating 3PCP, we assume that subsequent reversals remain on the same scanning curve until S_{imax} increases again.

For compositional changes to P_c, the same approach is advocated as used previously for k_r, based on the mass

fractions α_{gg} and α_{go}. However, we also need to take account of the change in IFT's, so we use:

$$P^c_{cwo}\left(S_w, S_g\right) = \alpha_{go}\sigma^r_{wg}P^m_{cwg} + \left(1-\alpha_{go}\right)\sigma^r_{wo}P^m_{cwo} \quad \text{..... (36)}$$

where:

$$\sigma^r_{wi} = \sigma_{wo}/\sigma^m_{wi} \quad \text{..... } i = g,o \quad \text{..... (37)}$$

and we approximate:

$$\sigma_{wo} = \alpha_{go}\sigma^m_{wg} + \left(1-\alpha_{go}\right)\sigma^m_{wo} \quad \text{..... (38)}$$

Eq. (38) should be reasonable, provided $\sigma^m_{wg} \approx \sigma^m_{wo}$. An equation similar to Eq.(36) applies for the hysteresis bounding curve P^c_{cow}. A compositional value for S^c_{ww} is then obtained from finding the cross over position $P^c_{cwo} = 0$. For P^c_{cgo} there are questions raised by the possibility of double displacement processes (c.f. Eq. 31), but we persevere with the usual assumption:

$$P^c_{cgo} = \left(\sigma_{og}/\sigma^m_{og}\right)P^3_{cgo} \quad \text{..... (39)}$$

When miscibility is approached, $P^c_{cgo} \to 0$.

Discussion

In the previous sections we have attempted to make compromises between the complexity of the models and the need to include the more essential physical aspects of 3P flow. A key consideration was to avoid the introduction of large numbers of unphysical parameters, and to retain as simple form of logic as this complex subject will allow. The latter has been served well by the success of the rescaled saturation interpolation method (RIM) for 3PRPs. Unfortunately, the only 3P measurement set for intermediate wet conditions available to us implies unattractive prospects for immiscible WAG injection, and more experiments are needed to confirm this trend. The success of RIM for matching measured isoperms gives encouragement to the use of simple interpolation methods for handling the effects of changes in phase compositions, and the convergence to the miscible limit. However, the consequent changes in the isoperm contours are quite large; we have not seen such results published previously and there is a need for research to validate the merits of this compositional treatment. We have also advocated the use of RIM to represent 3P k_{rw} and k_{rg}. The effects of hysteresis in 3PRPs are not adequately understood and we have made significant simplifying assumptions. In this regard, more information is needed on hysteresis effects for 2P k_r for mixed wet systems. Our models do not include at this stage a capability to deal with k_r which are cycle-dependent[11], and S_{wc}, S^m_{orw} and S^m_{org} are dealt with as constants. In practice, all the data can be made functions of material region, and if necessary conventional rescaling used to allow end points to change with absolute permeability, etc.

For 3PCPs we have placed reliance on a simple model for distributions of 3P-saturations under mixed-wet conditions. More elaborate models concerning the possible saturation distributions are arising from the research by van Dijke et al, but there does not appear to be an easy way to encapsulate this work in a general compositional framework. Another difficulty might be the additional measurements required for a meaningful reservoir application. Our proposals lead to strong effects in the consequent 3PCPs, and further significant changes arising from hysteresis and compositional affects. There do not appear to be any academic measurements to indicate the real trends. Inclusion of 3PCPs in compositional simulation is relatively new. Provided the gridding is fine enough to represent the saturation and compositional gradients, scoping numerical studies might reveal the level of importance of these approximations.

The proposed models given in this paper lead to a requirement to make additional measurements from those conventionally undertaken for 2PRPs and 2PCPs. The 2PRPs must include the full saturation range, and not omit values below a Buckley-Leveret front from a dynamic displacement experiment. We also suggest a need to undertake secondary water/oil drainage measurements from S_{orw} for bounding curves for both k_r and P_c under the appropriate reservoir wettability conditions. For the gas/oil system the primary drainage curve needs to be supplemented by a good measurement of S_{gtm} from secondary imbibition, and also the corresponding P_{cog} bounding curve. All the gas/oil measurements should be made with S_{wc} present, and the determination of S_{org} needs to be painstaking at a relevant capillary number. For the near miscible aspects, estimates are required for N_{goc}, the critical capillary number, and also for $S_{obw}(S_w)$, the water blocking function. We have not made a special provision for a miscible residual oil, since this can be included in S_{obw}.

Nomenclature

a = Parameter in equations for S_{om}
k_{rij} = Relative permeability of phase i relative to phase j
N = Capillary number
P_{cij} = Capillary pressure when phase i displaces phase j
r = Rescaling parameters
S = Saturation
S_{gw} = Interpolation weight
S_{obw} = Water blocking function
S_{of} = Rescaled oil saturation
S_{og} = Rescaled oil saturation to gas
S_{om} = Residual oil saturation
S_{ow} = Rescaled oil saturation to water
α = Parameter in equations for S_{om}
β = Parameter in equations for S_{om}
μ = Viscosity
ρ = Density
σ = Surface tension

Subscripts

c = Critical
g = Gas
h = Hydrocarbon
max = Maximum
min = Minimum
gr = Residual gas
gt = Trapped gas
o = Oil
org = Oil residual to gas.
orw = Oil residual to water.
w = Water
ww = Point of zero oil-water capillary pressure

Superscripts

3 = Three phase
c = Compositional mixed
h = Hysteresis or hydrocarbon
m = Measured
mi = Miscible or measured imbibition
md = Measured drainage
nm = Near miscible
r = Rescaled
rg = Rescaled to gas
ro = Rescaled to oil

Acknowledgements

The authors would like to thank BP Amoco for allowing this paper to be published, and especially Charles Christopher for his encouragement.

References

1. M. Haajizadeh, F.J. Fayers, A.P. Cockin, M. Roffey, and D.J. Bond: "On the Importance of Dispersion and Heterogeneity in the Compositional Simulation of Miscible Gas Processes", SPE 57264, presented at SPE Asia Pacific IOR Conference, Kuala Lumpar, Oct. 1999.
2. Johns, R.T., Fayers, F.J. & Orr, F.M. Jr.: "Effect of Gas Enrichment and Dispersion on Nearly Miscible Displacements in Condensing/Vaporizing Drives", SPE 24938, presented at SPE Annual Technical Conference, Washington DC, Oct. 1992.
3. Fayers F. J. and Mathews J.D.: "Evaluation of Normalised Stone's Methods for Estimating Three-Phase Relative Permeabilities", *SPE Journal*, April 1984, pp 224-232.
4. Balbinski, E.F. *et al*: "Key Characteristics of Three-Phase Oil Relative Permeability Formulations for Improved Oil Recovery Predictions", *Petroleum Geoscience* Vol 5, pp 339-346, 1999.
5. Baker, L.E., "Three-Phase Relative Permeability Correlations", SPE/DOE 17369 presented at the 1988 SPE/DOE Symposium on Enhanced Oil Recovery, Tulsa, April 17-20.
6. Hosain, A.: "Three-Phase Relative Permeability Measurements", MS Thesis, U. Birmingham, UK (1961).
7. Saraf, D.N. *et al*: "An Experimental Investigation of Three Phase Flow to Water/Oil/Gas Mixtures Through Water-Wet Sandstones", SPE 10761 presented at the 1982 SPE California Regional Meeting, San Francisco, March 24-26, 1982.
8. Oak, M.J.: "Three Phase Relative Permeability of Intermediate-Wet Berea Sandstone" SPE 22599 presented at the 66th Annual technical Conference and Exhibition of the SPE, Dallas, TX, October 6-9, 1991.
9. van Dijke, M.J.I *et al*: "A Process-Based Approach for Three-Phase Capillary Pressure and Relative Permeability Relationships in Mixed-Wet Systems", SPE 59310 to be presented at SPE/DOE Improved Oil Recovery Symposium held in Tulsa, Oklahoma, 3–5 April 2000.
10. Killough, J.E.: "Reservoir Simulation with History-Dependent Saturation Functions", SPE 5106 presented at the SPE-AIME 49th Annual Fall Meeting, Houston, Texas, Oct 6-9, 1974.
11 Christensen, J.R., Stenby, E.H., Lyngby and Skauge, A.: "Compositional and Relative Permeability Hysteresis Effects on Near-Miscible WAG", SPE 39627 presented at SPE/DOE Improved Oil Recovery Symposium, Tulsa, April 1998.

Appendix 1: Comments on Stone's Method I

Stone's Method I as it is commonly used is given by the equations :

$$k_{ro}\left(S_w, S_g\right) = S_o^* k_{row}^m\left(S_w\right) k_{rog}^m\left(S_g\right) \Big/ \left[k_{rocw}\left(1-S_w^*\right)\left(1-S_g^*\right)\right] \quad \text{.(A1)}$$

with:

$$\left.\begin{aligned} S_o^* &= \left(S_o - S_{om}\right)/\left(1 - S_{wc} - S_{om}\right) \\ S_w^* &= \left(S_w - S_{wc}\right)/\left(1 - S_{wc} - S_{om}\right) \\ S_g^* &= S_g/\left(1 - S_{wc} - S_{om}\right) \end{aligned}\right\} \quad \text{.....(A2)}$$

The linear form for the S_{om}-function[3] is usually employed:

$$S_{om}\left(S_g\right) = \alpha_g S_{org} + \left(1-\alpha_g\right) S_{orw} \quad \text{.....(A3)}$$

where

$$\alpha_g = S_g \Big/ \left(1 - S_{wc} - S_{org}\right) \quad \text{.....(A4)}$$

Eq. (A4) is slightly different from that used for RIM in Eq. (6), but the latter gives very similar results with $\beta = a = 0$. In Stone's I any form can be used for S_{om} which satisfies the limits S_{orw} and S_{org}. For RIM, the equation must ensure that the rescalings will satisfy the measured 2P k_r limits. In fact, Eq. (A4) implies S_{om} is a constant along lines where S_g is a constant, whereas Eq. (6) makes S_{om} a constant when $S_g/(S_w - S_{wc})$ is a constant. The latter seems more reasonable and possibly Stone's I would benefit from using the general form in Eqs. (5) and (6).

Perhaps the most surprising aspect about Eq.(A1) is the fact that k_{row} and k_{rog} are evaluated at S_w and S_g respectively, when S_o is likely to be the primary variable influencing 3P k_{ro}. In the 3P region, $S_o < 1 - S_w$ and $S_o < 1 - S_g$, hence the 2P k_r are evaluated at larger and inconsistent oil saturation. Using S_o as the look-up argument in the k_r gives unacceptable results. In particular we would then have $k_{ro} = 0$ when $S_o \le S_{orw}$. Eq. (A1) is linear in S_o through the factor S_o^*. The 2P k_{ri} functions

generally behave near their residuals like $k_{roi} \rightarrow \left(S_o - S_{ori}\right)^{n_i}$ with $n_i > 2$, i.e. distinctly non-linear near their residuals. Fig 1 shows how the consequent 3P isoperms close to S_{om} change their shape near the 2P limits. A more reasonable behavior close to S_{om} would be obtained through using $\left(S_o^*\right)^{n_o}$ with n_o interpolated between n_g and n_w based on a weighting like Eq. (A3). However, this would significantly change Stone's I k_{ro} at larger S_o. We also find that the latter can sometimes have the wrong curvature (see Fig 5). At large S_o the equation for S_{om} exerts only minor influence on Stone's I.

Appendix 2: Two Phase Relative Permeabilities

Relationships used for generating 2P curves for input to examples in this paper are the Chierici[2] type relationships:

$$k_{roi} = k_{rocw} \exp\left[- A_{oi} \left(\frac{S_i - S_{ip}}{S_{iq} - S_i} \right)^{\alpha_{oi}} \right]$$

$$k_{rio} = k_{riro} \exp\left[- A_i \left(\frac{S_i - S_{ic}}{S_{iq} - S_i} \right)^{-\alpha_i} \right]$$

for $i = w,g$, $S_{wq} = 1\text{-}S_{orw}$, $S_{gq} = 1\text{-}S_{org}\text{-}S_{wc}$, $S_{gp} = 0$ and $S_{wp} = S_{wc}$. The parameter values are given in Table 1.

	Field 1	Field2	Saraf et al	Hosain	Oak
S_{wc}	0.2	0.25	0.246	0.15	0.1
S_{orw}	0.17	0.245	0.4	0.15	0.27
S_{gc}	0.038	0.0	0.0	0.10	0.03
S_{org}	0.07	0.205	0.326	005	0.28
K_{rocw}	0.967	1.0	0.85	0.88	0.8
K_{rwro}	0.714	0.4	0.075	0.5	0.7
K_{rgro}	0.914	0.5	0.357	0.58	0.63
A_w	2.717	1.047	2.281	1.323	2.612
α_w	1.066	0.512	0.845	0.651	0.830
A_{ow}	3.002	2.906	0.906	1.644	2.024
α_{ow}	0.879	0.6	0.773	0.637	0.709
A_g	0.999	1.349	2.794	1.837	1.430
α_g	1.168	0.647	0.601	0.617	1.093
A_{og}	5.324	2.314	1.279	2.320	2.418
α_{og}	0.894	0.710	0.792	0.849	0.860

Table 1 - Parameterisation of Two Phase Relative Permeability Curves

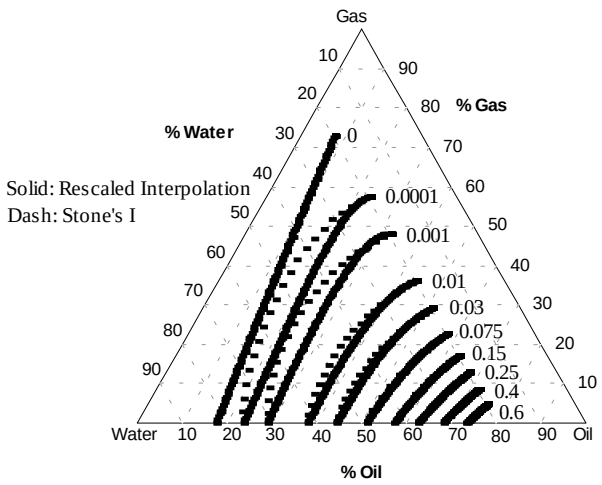

Figure 1 - Rescaled Interpolation versus Stone's I Isoperms (Field 1)

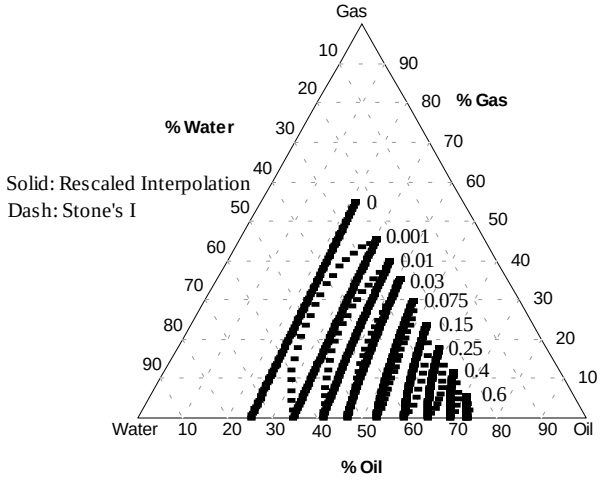

Figure 2 - Rescaled Interpolation versus Stone's I Isoperms (Field 2)

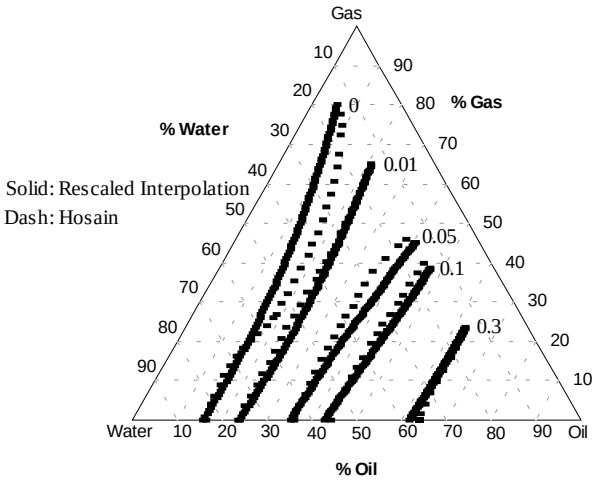

Figure 3 - Rescaled Interpolation versus Hosain Isoperms

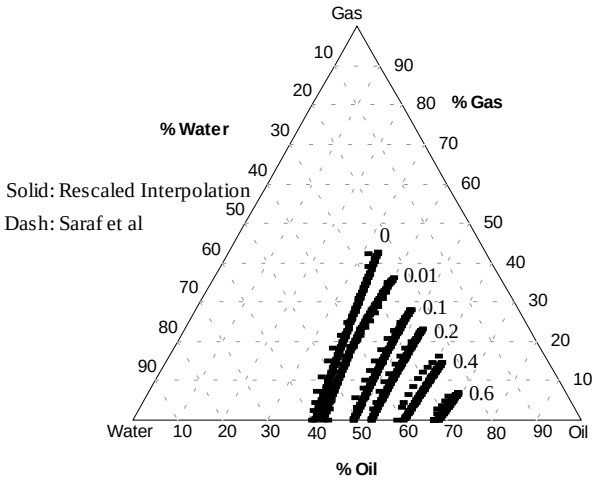

Figure 4 - Rescaled Interpolation vs Saraf et al Isoperms

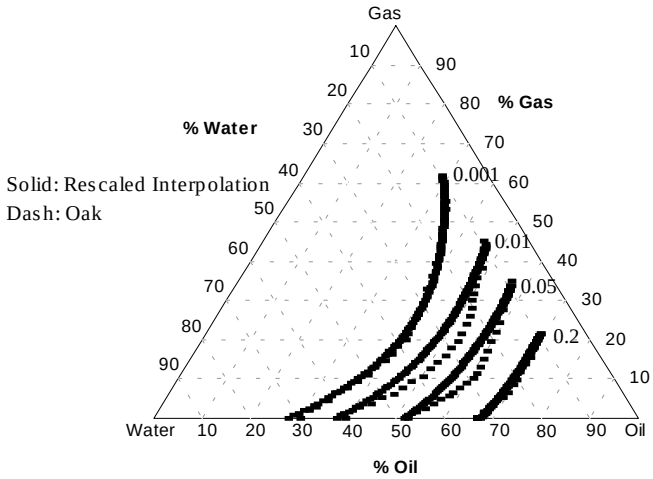

Figure 5a - Rescaled Interpolation Method

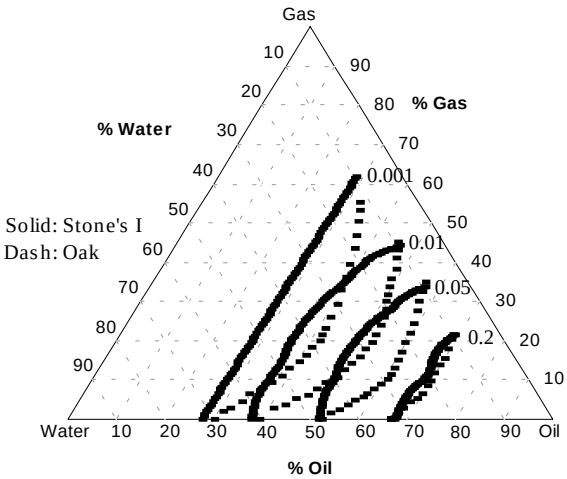

Figure 5b - Stone's I

Figure 5 - Rescaled Interpolation Method and Stone's I versus Oak Isoperms

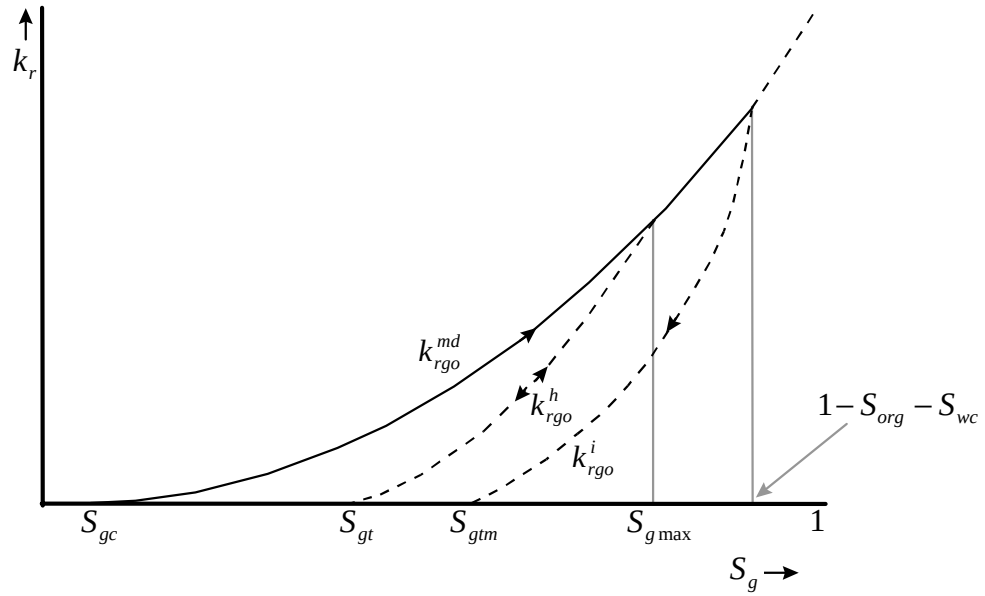

Figure 6 - Hysteresis in Gas-Oil Relative Permeability

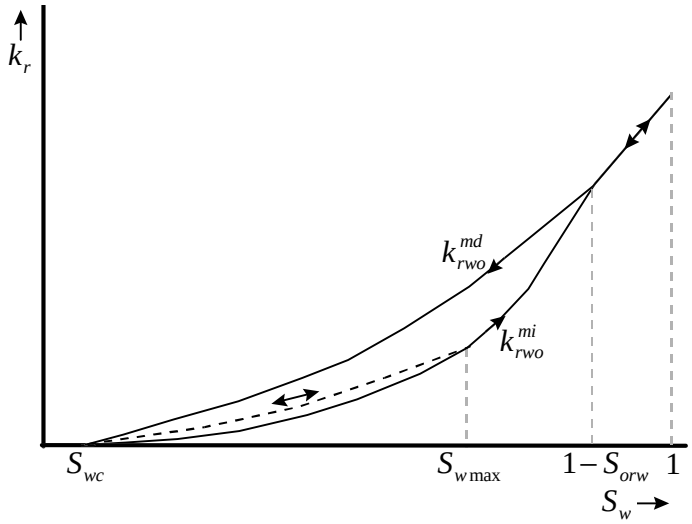

Figure 7a - Water Relative Permeability

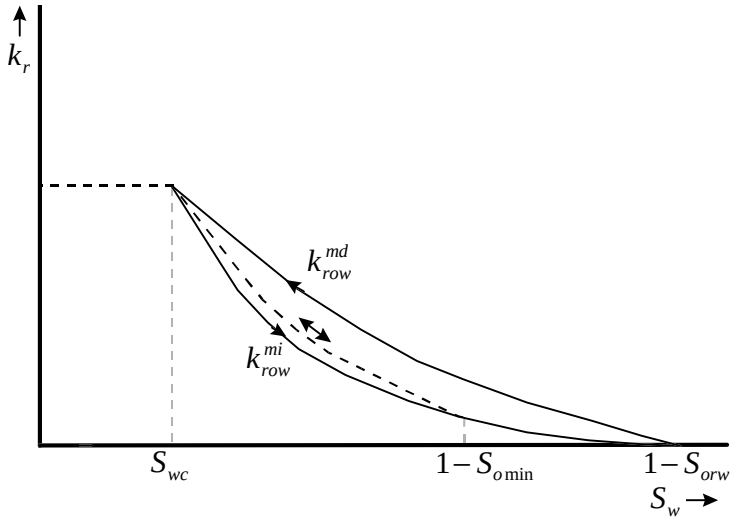

Figure 7b - Oil Relative Permeability

Figure 7 - Water and Oil Relative Permeability Hysteresis

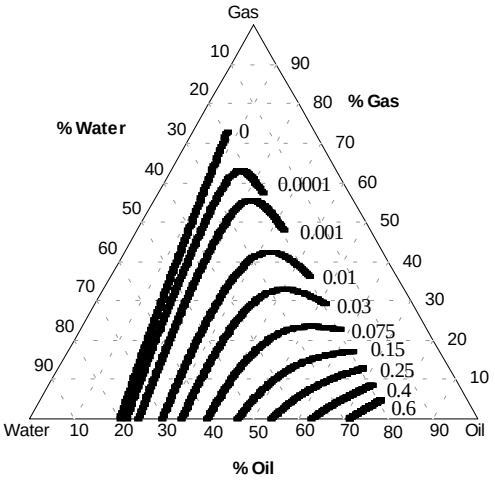

Figure 8 - Composition-Dependent Oil Isoperms (Field 1)

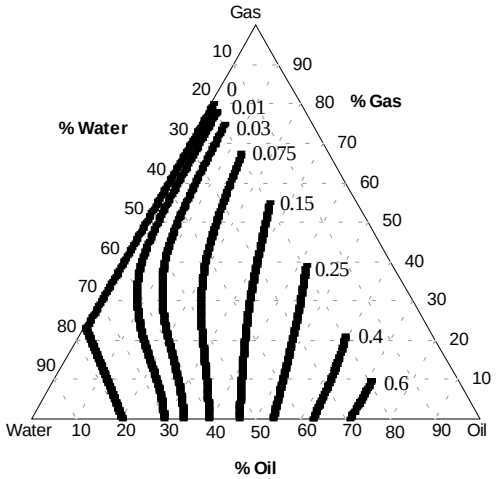

Figure 9 - Predicted Near-Miscible Oil Phase Isoperms (Field 1)

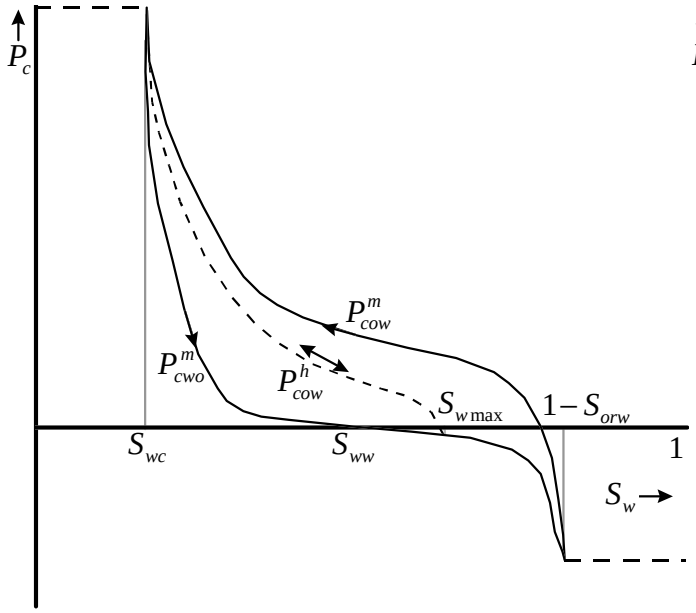

Figure 10a - Water-Oil

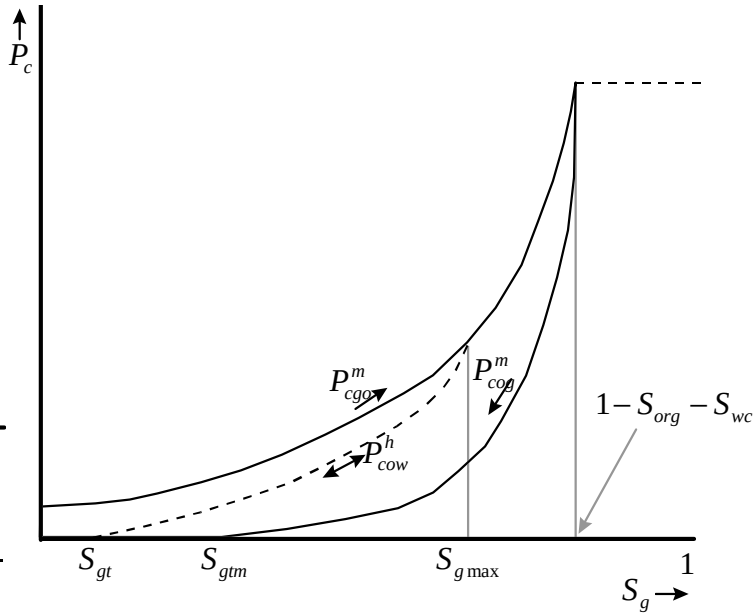

Figure 10b - Gas-Oil

Figure 10 - Capillary Pressure Curves

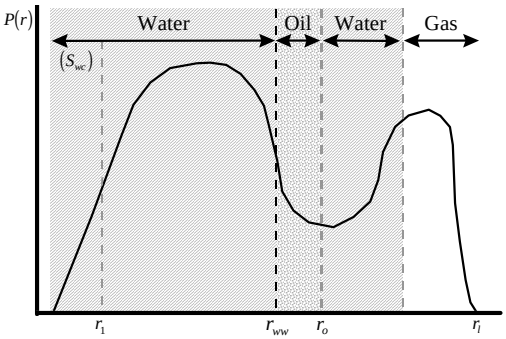

Figure 11a - Three Phase

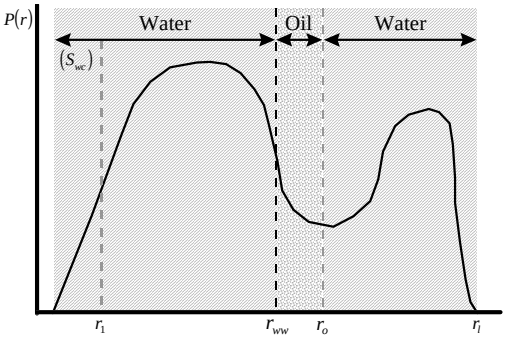

Figure 11b - Two Phase (Water-Oil)

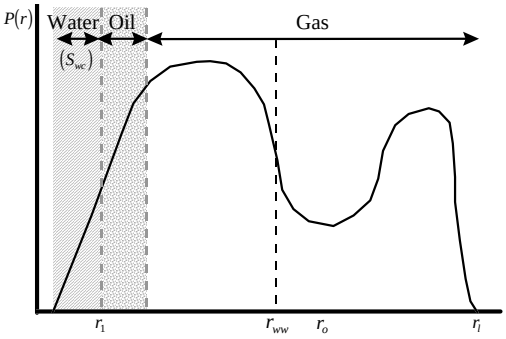

Figure 11c - Two Phase (Gas-Oil)

Figure 11 - Saturation Distributions When $S_w > S_{ww}$ with S_o as the Look-Up Variable

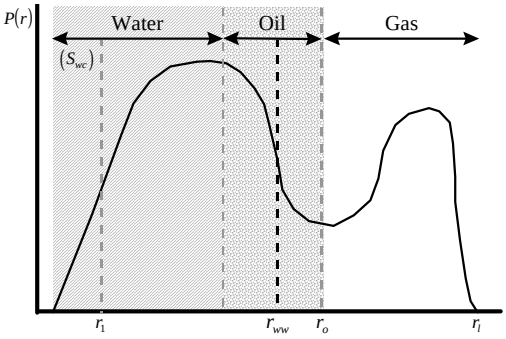

Figure 12a - Three Phase

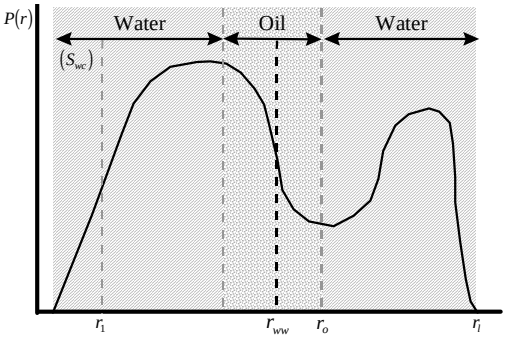

Figure 12b - Two Phase (Water-Oil)

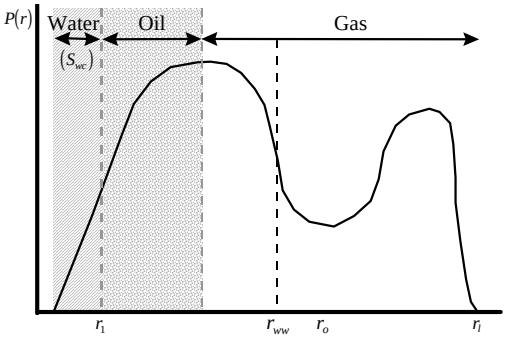

Figure 12c - Two Phase (Gas-Oil)

Figure 12 - Saturation Distributions When $S_w < S_{ww}$ with S_o as the Look-Up Variable

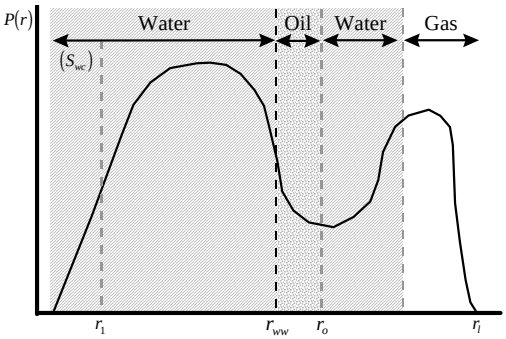

Figure 13a - Three Phase

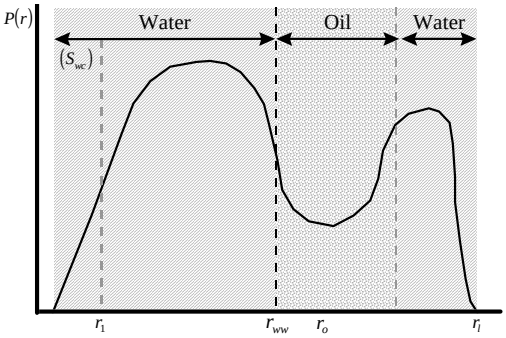

Figure 13b - Two Phase (Water-Oil)

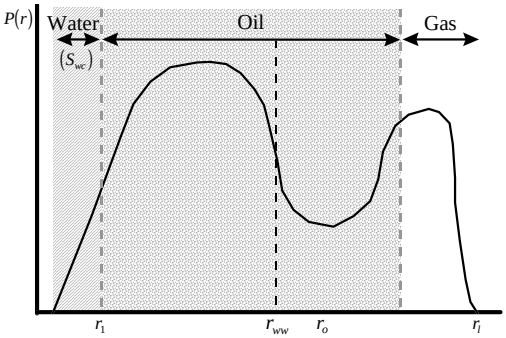

Figure 13c - Two Phase (Gas-Oil)

Figure 13 - Saturation Distributions When $S_w > S_{ww}$ with S_w and S_g as the Look-Up Variables

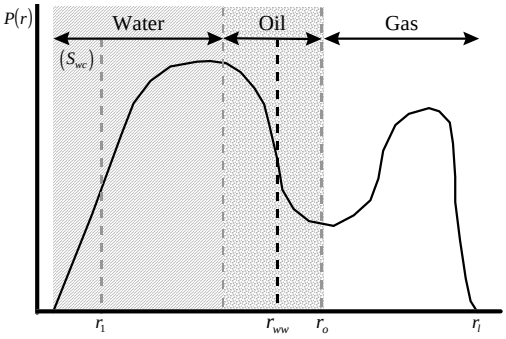

Figure 14a - Three Phase

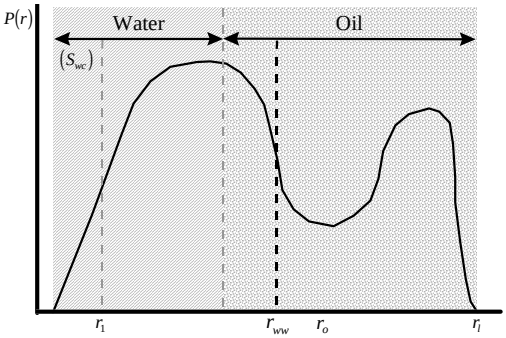

Figure 14b - Two Phase (Water-Oil)

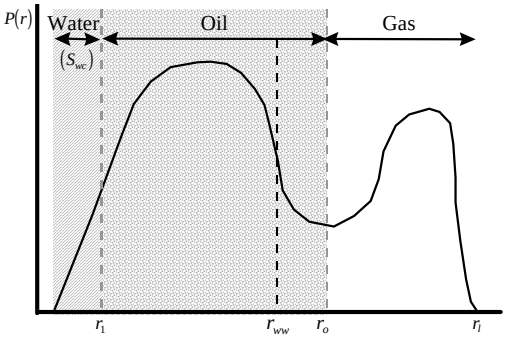

Figure 14c - Two Phase (Gas-Oil)

Figure 14 - Saturation Distributions When $S_w < S_{ww}$ with S_w and S_g as the Look-Up Variables

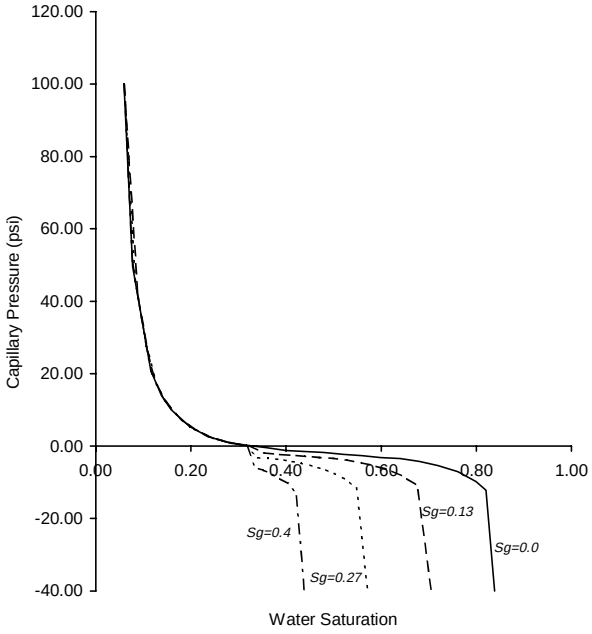

Figure 15a: Water-Oil

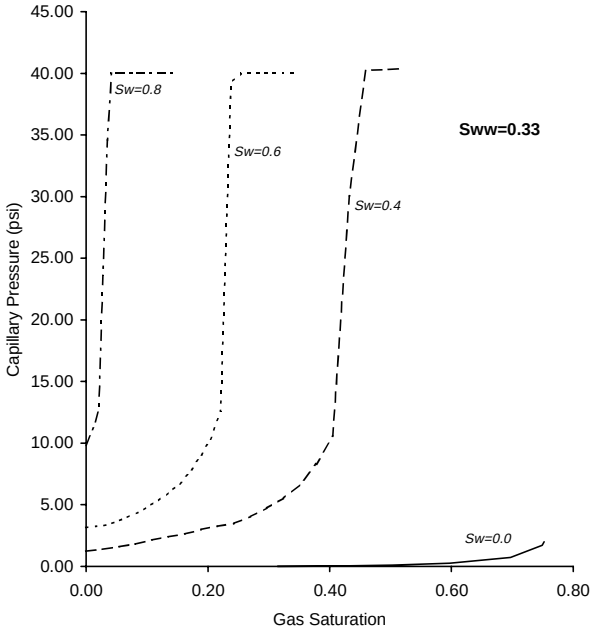

Figure 15b: Gas-Oil

Figure 15 - Three Phase Capillary Pressures